4-24-2020

Multi-Attribute Analysis Using Coherency and Ant-Tracking Techniques for Fault and Fracture Detection in La Florida Anticline, Llanos Foothills, Colombia

Ziyad Albesher

James N. Kellogg

Ibraheem Hafiza

Essam Saeid

geosciences

MDPI

Article

Multi-Attribute Analysis Using Coherency and Ant-Tracking Techniques for Fault and Fracture Detection in La Florida Anticline, Llanos Foothills, Colombia

Ziyad Albesher [1,2,*], James Kellogg [1], Ibraheem Hafiza [1,2] and Essam Saeid [1,3]

[1] The School of the Earth, Ocean and Environment, University of South Carolina, Columbia, SC 29208, USA; Kellogg@sc.edu (J.K.); ihafiz@email.sc.edu (I.H.); esaeid@email.sc.edu (E.S.)
[2] King Abdulaziz City for Science and Technology (KACST), Riyadh 12354, Saudi Arabia
[3] Department of Earth Sciences, University of Benghazi, Benghazi, Libya
* Correspondence: albesher@email.sc.edu

Received: 2 April 2020; Accepted: 22 April 2020; Published: 24 April 2020

Abstract: We present techniques to reduce noise and enhance seismic quality, making possible the first multi-attribute analysis of a 3D seismic volume in the Llanos Foothills (La Florida anticline) of Colombia using coherency and ant-tracking techniques for fault and fracture detection. The results could help reduce risk in models of reservoir fracture porosity and permeability. The dominant fracture strike direction in the studied seismic volume (La Florida anticline) is NE–SW (055 ± 20°), parallel to the structural strike of the adjacent Eastern Cordillera Foothills. The application of the ant-tracking technique also reveals the NE-SW fracture set for the reservoir rocks in the La Florida anticline as well as in the non-folded reservoir rocks to the SE. We compared the fracture intensity and orientation in folded rocks with the fracture intensity and orientation in non-folded rocks. Our study showed NE-SW, NW-SE, and E-W fracture orientations in the non-folded seismic volume, suggesting that regional stresses could produce these fracture sets, not just folding processes as previously proposed. The NW-SE and WNW-ESE fracture sets are only found in the Guayabo Formation (11 Ma–Present). A right–lateral strike–slip displacement on the nearby Algeciras fault system in the last 2 m.y. may have generated WNW-ESE and NW-SE Riedel-type shear fractures in the study area.

Keywords: Llanos foothills; La Florida anticline; attribute analysis; ant-tracking; fractures

1. Introduction

The La Florida anticline is located in the Llanos foothills on the southeastern flank of the Eastern Cordillera of Colombia (Figure 1) bounded by the Cusiana thrust fault system and the Llanos basin to the southeast, and by the Guaicaramo fault system and the Eastern Cordillera to the northwest. The eastern foothills contain important oil fields in a complex foreland fold and thrust belt (e.g., [1,2]). The main reservoirs of the giant Cusiana oilfield, the Mirador, Barco, and Guadalupe formations, have low porosity but are highly fractured in the fold traps [1,3]. Fracture systems are critically important for creating secondary porosity as well as pathways for hydrocarbon migration and production [1,3–5].

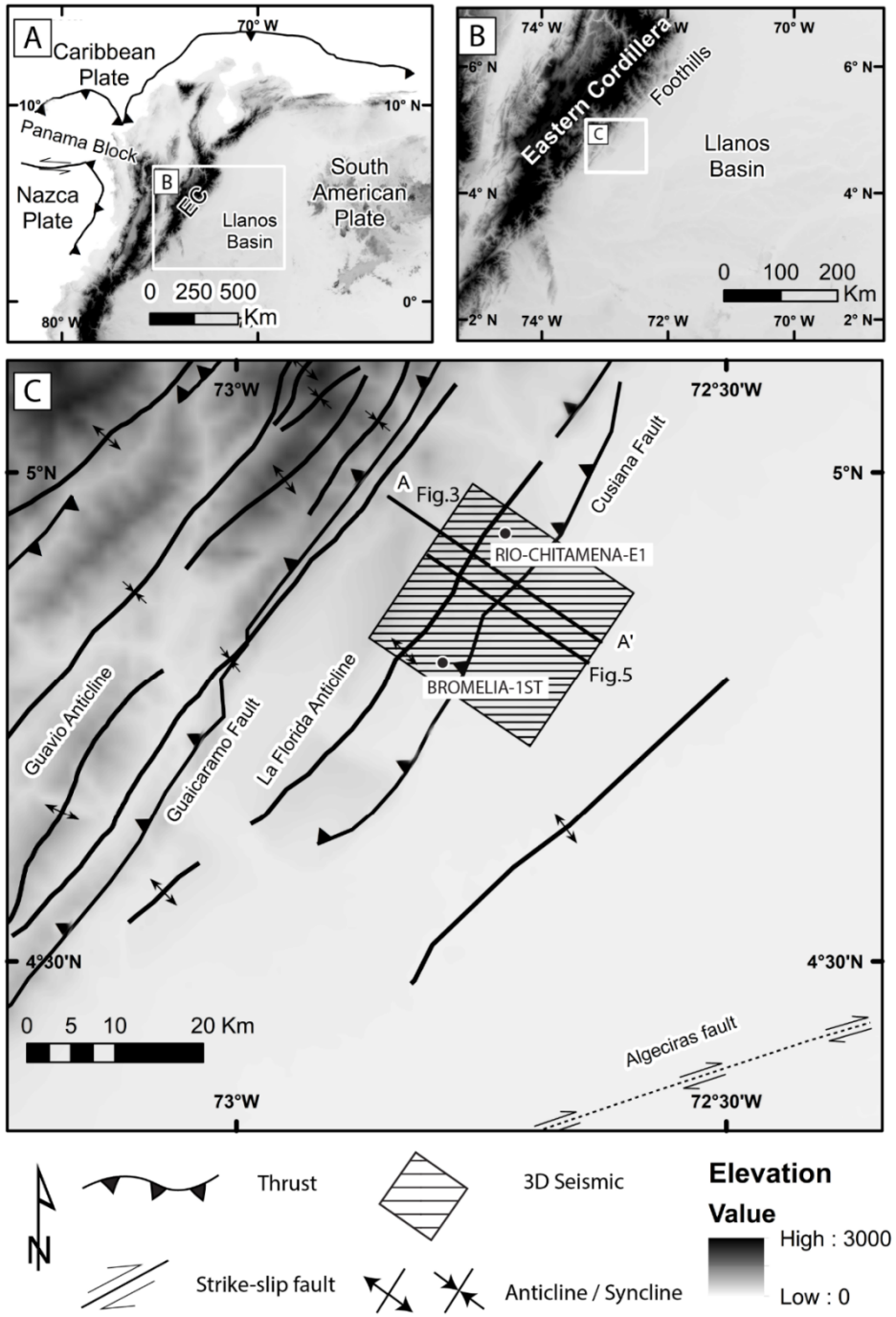

Figure 1. Shaded relief maps for (**A**) northwest South America, (**B**) Eastern Cordillera, and (**C**) structural features for the study area.

The La Florida anticline (Figure 1) is located on the trend of anticlinal traps associated with the Yopal–Cusiana fault system, including Rio Chitamena 3 km to the northeast and the giant Cusiana oilfield 16 km to the northeast [1]. Mora et al. (2010) [6] interpreted the La Florida anticline as being produced by slip on the Cusiana fault, a listric high angle reverse fault. Both Cooper et al. (1995) [2] and Cazier et al. (1995) [1] also interpreted the Cusiana fault as a listric reverse fault involving Early Cretaceous and older basement. Albesher et al. (2019) [7] reinterpreted all the thrusting on the Cusiana fault and La Florida anticline as thin-skinned and presented the first retrodeformed model for the La Florida anticline, proposing a previously unrecognized late Miocene–Pliocene fault-bend fold formed by a thin-skinned thrust ramping up from a mid-Cretaceous detachment.

Previous studies of fracture systems in the Eastern Cordillera Foothills related their distribution to fold types and geometries based on field mapping and subsurface borehole imager logs. Seismic attribute analysis has not been commonly used in foothills studies, because it is sensitive to high noise levels in the seismic data produced by strong deformation and high topographic relief. In this paper, we present techniques to reduce noise and enhance seismic quality, making possible the first multi-attribute analysis of a 3D seismic volume in the Foothills using coherency and ant-tracking techniques for fault and fracture detection. Because we were able to image a non-folded seismic volume for fractures, we could identify fractures produced by regional stress fields apart from folding processes. Furthermore, we studied a post-rift sedimentary volume from the Late Cretaceous to Present, and we were able to make some inferences about the relative timing and orientation of regional fracture sets. The results could help reduce risk in models of reservoir fracture porosity and permeability.

2. Geological Setting

2.1. Stratigraphic Setting and Petroleum System

The Llanos foothills separate the Eastern Cordillera from the Llanos basin and constitute a modern foredeep in the foreland basin system [8]. The sedimentary sequence in the Llanos foothills basin study area and adjacent Guavio anticline (Figures 1 and 2) is up to 12 km thick, including at least 6 km of Cenozoic synorogenic sediments [9,10]. The stratigraphic column (Figure 2), after Cooper et al. (1995) [2], Ramon and Fajardo (2006) [11], and Parra et al. (2009b) [9], shows the Llanos foothills oil system, and post-rift and foreland basin sedimentation. The basement is composed of Paleozoic metamorphic rock overlain by Albian–Cenomanian sandstones of Une Formation deposited during Late Cretaceous post-rift thermal subsidence. The Turonian–Santonian Gacheta Formation, the main source rock in the area, was deposited as thermal subsidence continued [12]. The Gacheta Formation was overlain by shallow marine sandstones and interbedded mudstones of the Campanian–Maastrichtian Guadalupe Group, a deep valuable reservoir in the Cusiana oilfield [1]. The second important reservoir in the Llanos foothills is a fluvial sandstone of the Paleocene Barco Formation. The Guadalupe Group reservoir is sealed by the Upper Paleocene mudstone of the Los Cuervos Formation [13,14]. The Eocene sandstones of the Mirador Formation are the main reservoir that preserve more than half of the hydrocarbons in the Llanos foothills and are considered the most important oil exploration target [11]. The late Eocene to early Miocene Carbonera Formation comprises interlayered transgressive shales and sandstone intervals, with the lower muddy interval C8 (Figure 2) forming the regional top seal for the underlying Mirador Formation (Fm) reservoir [11]. The shaly middle Miocene Leon Formation deposition coincided with uplift of the Eastern Cordillera that isolated the Llanos basin from the Magdalena Valley [2]. The Miocene–Holocene Guayabo Formation coarse-to-fine fluvial gravels interbedded with variegated floodplain deposits were produced by the rapid late Miocene Andean uplift [15].

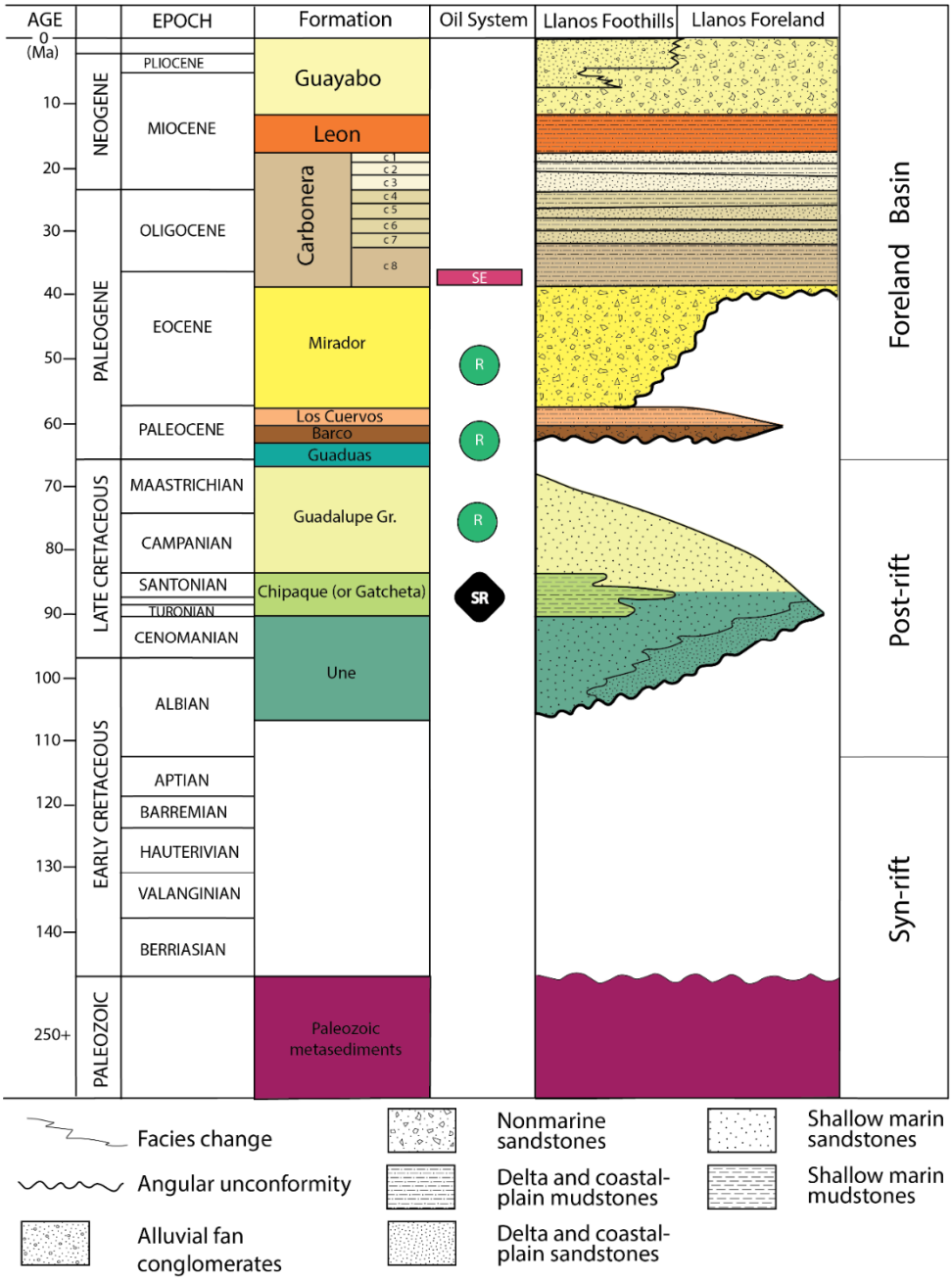

Figure 2. Chronostratigraphic diagram of Paleozoic–Cenozoic strata in the Llanos foothills (after Ramon and Fajardo, 2006; Parra et al., 2009).

2.2. *Structural Evolution of La Florida Anticline*

The La Florida anticline (Figure 1) was formed in the last 7 million years (Myr) by displacement on the underlying Cusiana thrust fault and the nearby Guaicaramo fault [8,16]. Mora et al. (2010) [6] interpreted the La Florida anticline as produced by slip on the Cusiana fault, a listric high angle reverse fault involving pre-Late Cretaceous basement rocks. Cooper et al. (1995) [2] and Cazier et al. (1995) [1] interpreted the Cusiana fault as an inverted listric normal fault involving Early Cretaceous and older basement. The total slip on the Cusiana high angle reverse fault is over 4 km [1]. Based on thermochronometric data and kinematic restorations, Bande et al. (2012) [17] and Carrillo et al. (2016) [16] suggest that the folds associated with the Cusiana fault originated in the last 3 Myr. Mora et al. (2010) [6] also noted that Pliocene–Pleistocene units on the back-limb of the Florida anticline are folded

conformably with no significant growth strata. None of these interpretations, however, explained the Cusiana hanging wall anticline.

Albesher et al. (2019) [7] used higher resolution seismic data than previous studies and were able to image the deeper anticline in the Mirador Formation as well as the detachment in the lower Carbonera Formation. Albesher et al. (2019) [7] also presented the first retrodeformed model for the La Florida anticline (Figure 3). They reinterpreted the thrusting on the Cusiana fault and La Florida anticline as thin-skinned. Their model also explained the La Florida anticline as a previously unrecognized late Miocene–Pliocene fault-bend fold formed by a thin-skinned thrust ramping up from a mid-Cretaceous detachment (Figure 3B). The fault-bend fold formed an early potential hydrocarbon trap. This was followed by thrusting on the Cusiana reverse fault, a forelimb breakthrough fault ramping up from two bedding plane faults in the Late Cretaceous Une Formation and in the Oligocene lower Carbonera Formation (Figure 3C). The total late Miocene–Pliocene shortening on the La Florida anticline was about 5.7 km.

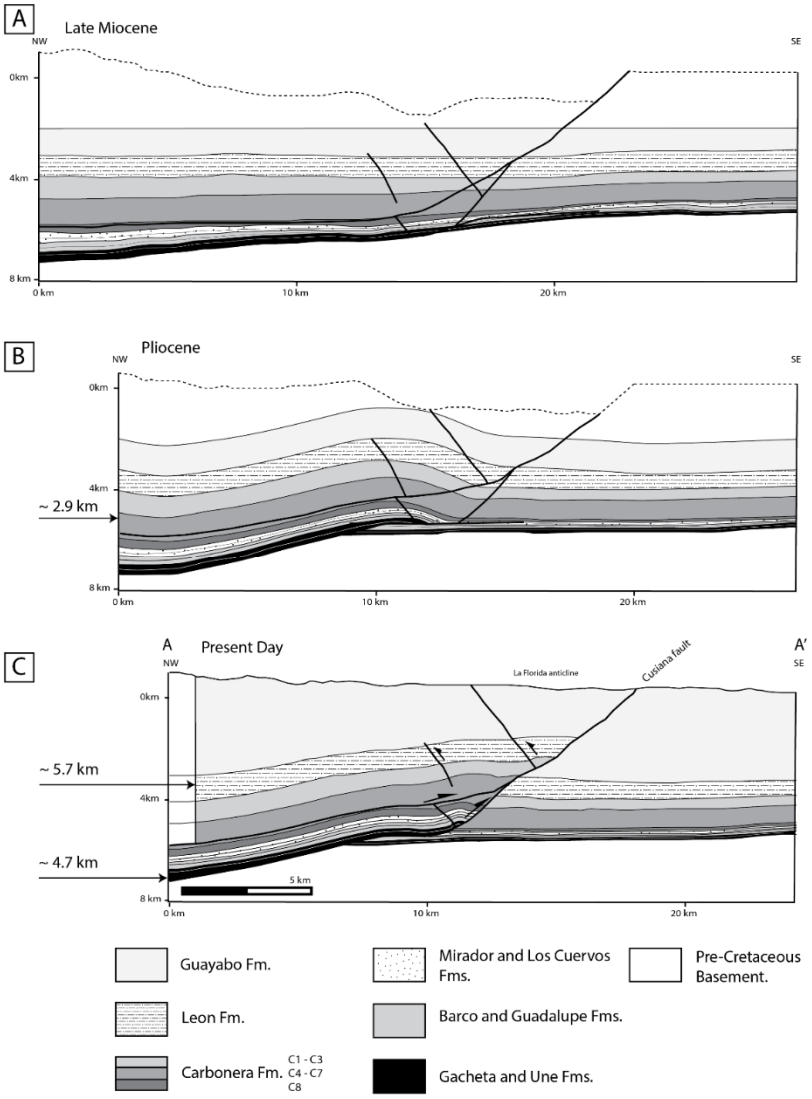

Figure 3. Retrodeformed model of the La Florida anticline (Albesher et al., 2019) during (**A**) late Miocene, (**B**) Pliocene, and (**C**) present time, respectively. See the location in Figure 1.

2.3. Previous Fracture Analysis in Foothills and Cusiana

Fractures may enhance permeability in reservoirs, increasing productivity and recovery efficiency [18]. In the Llanos foothills, Cazier et al. (1995) [1] found that the Eocene Mirador

Fm (the main reservoir) has a low porosity but good permeability in the giant Cusiana oilfield northeast of the La Florida anticline. Well tests indicated that the type of permeability was primarily matrix related [1]; however, fluid flow is likely also influenced by augmented fracture permeability [19]. Tamara et al. (2015) [3] studied the fracture systems in the Cusiana anticline using subsurface well data. They divided the Cusiana anticline into three segments, documented four fracture systems (NE–SW, NW–SE, E–W, and N–S) and related their distribution and intensity to fold geometry and folding mechanisms. They noted that the NE–SW fracture set was present everywhere in the Cusiana reservoir rocks, with high intensities in the hinge region of the anticline. They also correlated the general fracture distribution with changes in the structural style in the Cusiana anticline along strike. Their study was also based on the field mapping of outcrops in the Foothills to determine the relative timing of fracture sets, as well as using subsurface borehole imager logs for the Cusiana, Cupiagua, and Piedemonte oil fields.

Small faults not detected in traditional seismic reflection data may also cut migration pathways and reduce fluid pressure in basin models [20]. Seismic attributes can detect cracks and low displacement faults that are difficult to see in seismic amplitude data. In this study, we use geometric attributes, especially the reflector continuity edge detect tool "coherence" [21]. Image log analysis, a traditional method for detecting subsurface fractures, is reliable and derived from direct observation. It is limited to wells where image logs are available and does not sample the rock volume between wells. In this study, we took advantage of a high-resolution 3D seismic volume and applied the swarm intelligence algorithm attribute, known commercially as ant-tracking [22]. In the Sabriyah oil field (northern Kuwait), Singh et al. (2008) [23] showed that the ant-tracker attribute effectively detected fracture orientations and provided similar results to fracture orientations found in well image logs. We note that results extracted from the La Florida seismic volume by ant-tracking attributes in this study are also similar to those obtained in reservoir rocks from the nearby Cusiana wells [3].

3. Research Methods

3.1. Post-Migration Data Conditioning and Image Enhancement

Synthetic seismograms were created for the Rio Chitamena and Bromelia wells along the 3-D seismic volume of the La Florida anticline (see Figure 1 and Figure 6 for locations). The Rio Chitamena well constrained the northern part of the Cusiana thrust hanging wall, and the Bromelia well constrained the Cusiana footwall to the south. Well logs were used to create synthetic seismogram traces. The seismic cross-sections were then tied to the wells using velocities from well check-shot surveys and adjusting the time–depth function by stretching and squeezing the wavelet until the seismic matched the synthetic seismogram (Figure 4). The Eocene Mirador Formation (the main reservoir in the Llanos foothills) reflectors can be seen at 2.34 to 2.39 s TWT in the Rio Chitamena well in the hanging wall (Figure 4).

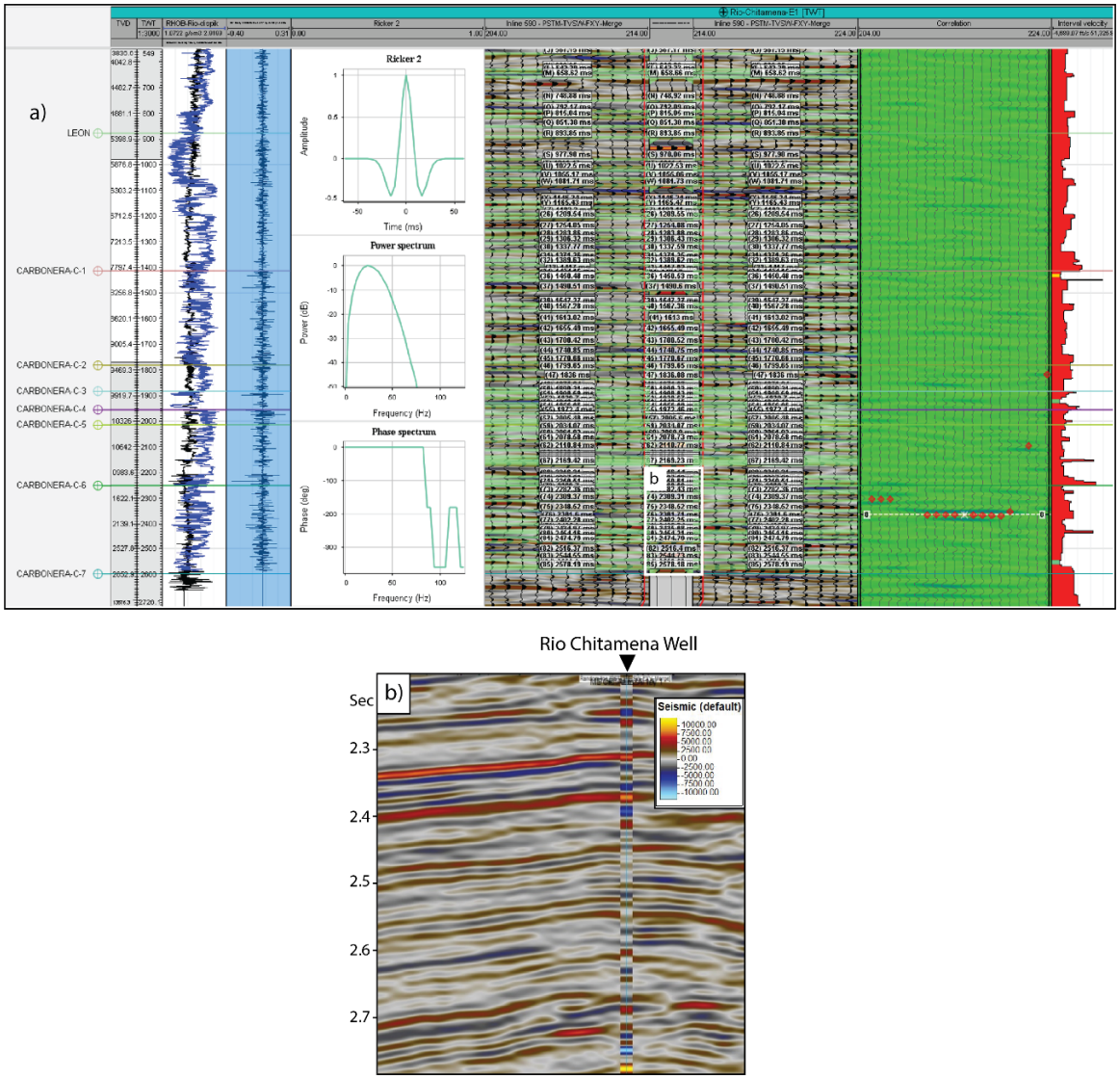

Figure 4. (**a**) Synthetic seismogram with sonic and density logs. (**b**) Synthetic seismogram for the Rio Chitamena well displayed on a seismic section.

The interpretation of critical features such as faults and fractures in seismic amplitude data is complicated in the Foothills by noise introduced to the data by structural and topographic complexity. Randen et al. (2003) [24] suggested a way to suppress the noise by applying a "structure-oriented filter", using the principles of scale-space theory to smooth the seismic volume and detect geological features at different stages of resolution. Depending on the feature of interest, large smoothing (increasing the continuity of the seismic reflectors) leaves primarily major features like thrust faults, while low smoothing leaves minor features [24]. Figure 5 shows the effects of using the structure smoothing filter on our 3D seismic volume, where the resolution was increased by enhancing the horizontal continuity of the seismic reflectors. The structure smoothing filter decreases the data noise level and makes an accurate seismic attribute analysis possible.

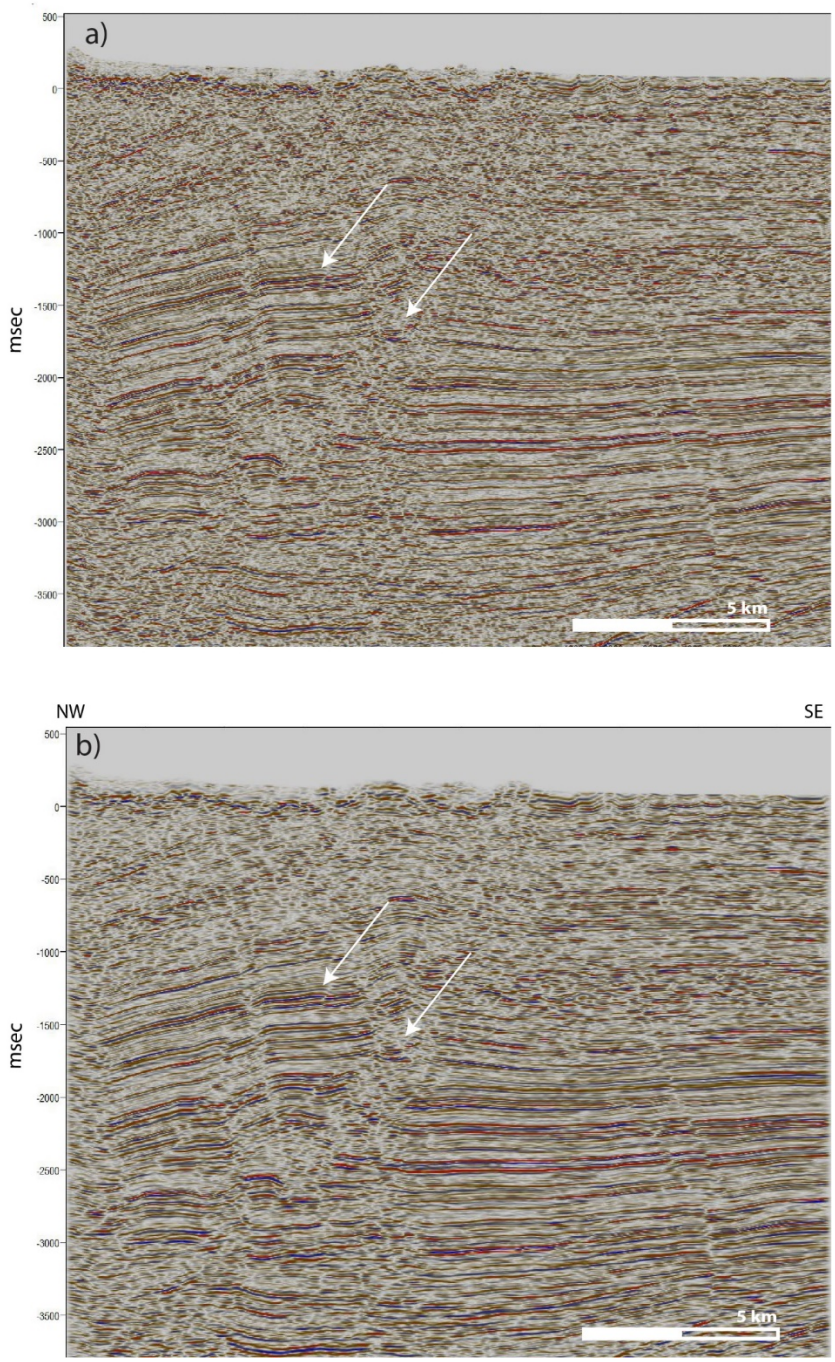

Figure 5. (**a**) Amplitude seismic cross-section before applying the structure smoothing filter, and (**b**) after applying the structure smoothing filter. The white arrows indicate areas of increased reflector resolution and reduced noise near the Cusiana fault plane after filtering in Figure 5b. For the profile location, see Figure 1.

3.2. Coherence and Ant-Tracking Seismic Attribute Analysis

A seismic attribute is a measurement derived or extracted from seismic data [22], which helps to visually enhance or focus on the geological features of greatest interest. The optimal results from seismic attributes depend on data conditioning and the quality of the seismic data. Deformation in the Llanos Foothills is intense, especially in the northeast where it is difficult to apply seismic attribute analysis because of the deformation noise. Fortunately, the La Florida structure is a gentle anticline [6,7,15], and the La Florida footwall is relatively undeformed, which means that we are able to

apply seismic attribute analysis to the La Florida 3D seismic volume (Figure 6). For this study, we used Petrel 2019.3 software from Schlumberger for the seismic interpretation, and we produced the seismic attributes by following the fault imaging workflow (Figure 7).

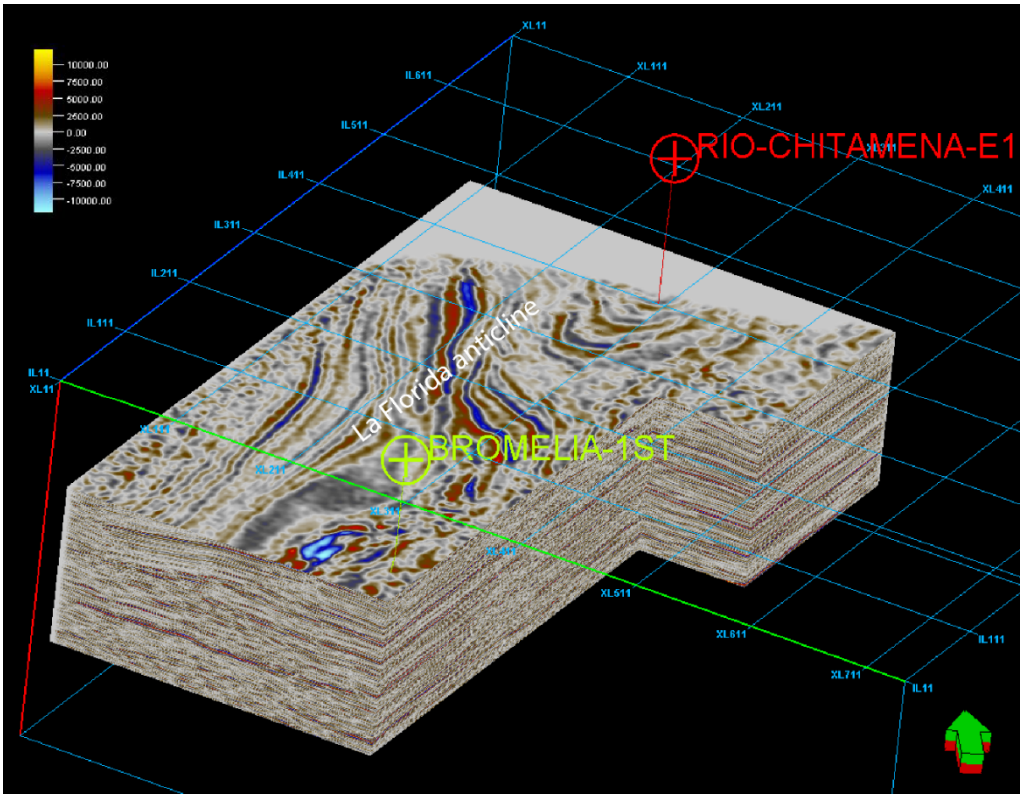

Figure 6. 3D Seismic amplitude volume of the La Florida anticline showing the well locations.

The coherence attribute enhances the ends of reflectors, where these edges can delineate faults or even fault damage zones in fractures [21]. This application mainly measures the lateral changes in waveform and amplitude [22], and therefore coherence can enhance lateral resolution and produce a relatively sharp definition for faults and fractures [18]. For that purpose, we applied the coherence attribute on the 3D seismic cube after applying the structure smoothing filter to reduce noise and extract faults and fractures that are not readily visible in the seismic amplitude data.

Ant-tracking is an advanced attribute that uses the swarm intelligence algorithm to enhance discontinuities [25]. The ant-trackers' mission (i.e., artificial ants) is to find all the discontinuity traces in three dimensions inside the 3D coherence attribute volume and enhance those minor/weak traces that represent possible small faults or fractures. Using this approach, we set azimuthal parameters (the azimuth filter is a tool to control the moving direction of ant-trackers inside the 3D coherence volume) before allowing the "artificial ants" to search for discontinuities in the edge-detection volume. We first force the ant-trackers to search in all directions by applying all azimuths at $-180° < \phi < 180°$ to capture features that are continuous and likely to be faults and to ignore other features with a short continuity such as noise or channels. Therefore, the first result will show faults and fracture zones from all azimuths distributed throughout the whole volume. In the second step, we use an azimuthal filter to hide the dominant fracture orientation and allow the ants to search in the remaining directions to detect secondary faults and fractures that may have been hidden. Finally, 3D visualization of faults and fractures in the ant-tracking attribute volume prepares the data for automatic fault extraction [25]. The fractures can then be displayed as dip azimuth points and strike azimuth rose diagrams [26].

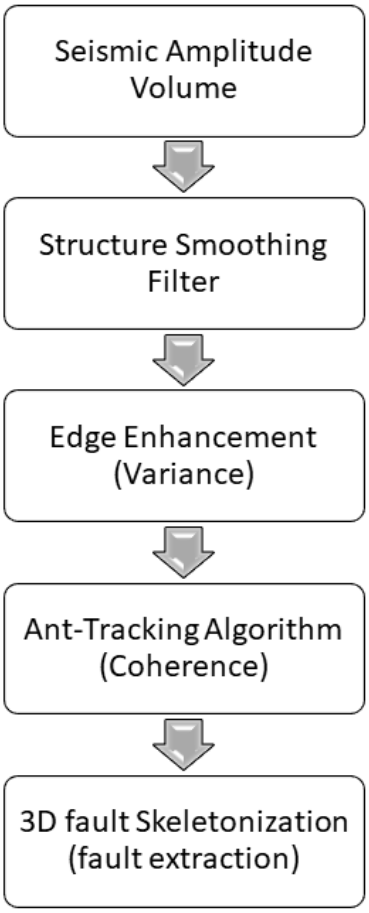

Figure 7. Workflow illustrating the steps used in our attribute analysis, which involved the generation of ant-tracking and fault extraction volumes.

4. Results

4.1. 3D seismic Visualization of the La Florida Anticline

Figure 8a shows the ant-tracking results for the La Florida 3D seismic volume, including the Cusiana fault hanging wall and footwall. Parameters and filters were applied to the ant-tracking volume to reduce the signal of non-fracture features, such as channels and bedding. For example, we only mapped fracture patches dipping over 75 degrees to filter out bedding plane effects. Figure 8b shows the fault and fracture patches for the 3D ant-tracking volume with no azimuthal filter applied. The fault patches volume clearly shows a greater fracture intensity in the folded Cusiana hanging wall than in the non-folded footwall. One way to quality control (QC) the ant-tracking fault and fracture patch predictions is to compare them to structural features in the seismic amplitude volumes. Figure 9 is a 3D window showing an ant-tracker time slice and a seismic reflection profile. The white arrows point to faults or fractures visible in the seismic amplitude vertical section that match fractures predicted in the ant-tracker time slice.

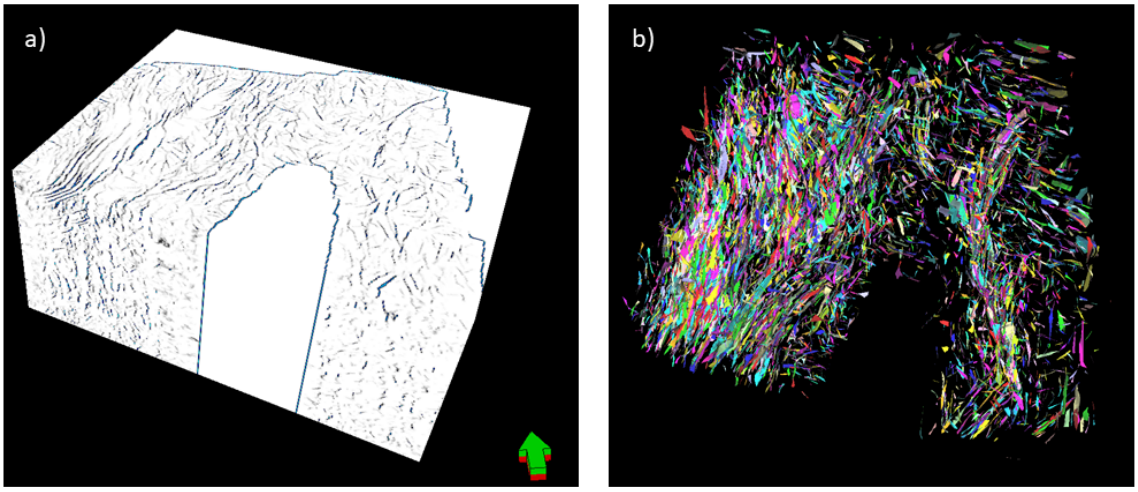

Figure 8. (**a**) The Ant-tracking results for the whole 3D seismic volume including the La Florida anticline (left side) and the Cusiana fault footwall block (right side). (**b**) The fault patches volume shows a greater fracture intensity in the folded Cusiana hanging wall than in the footwall.

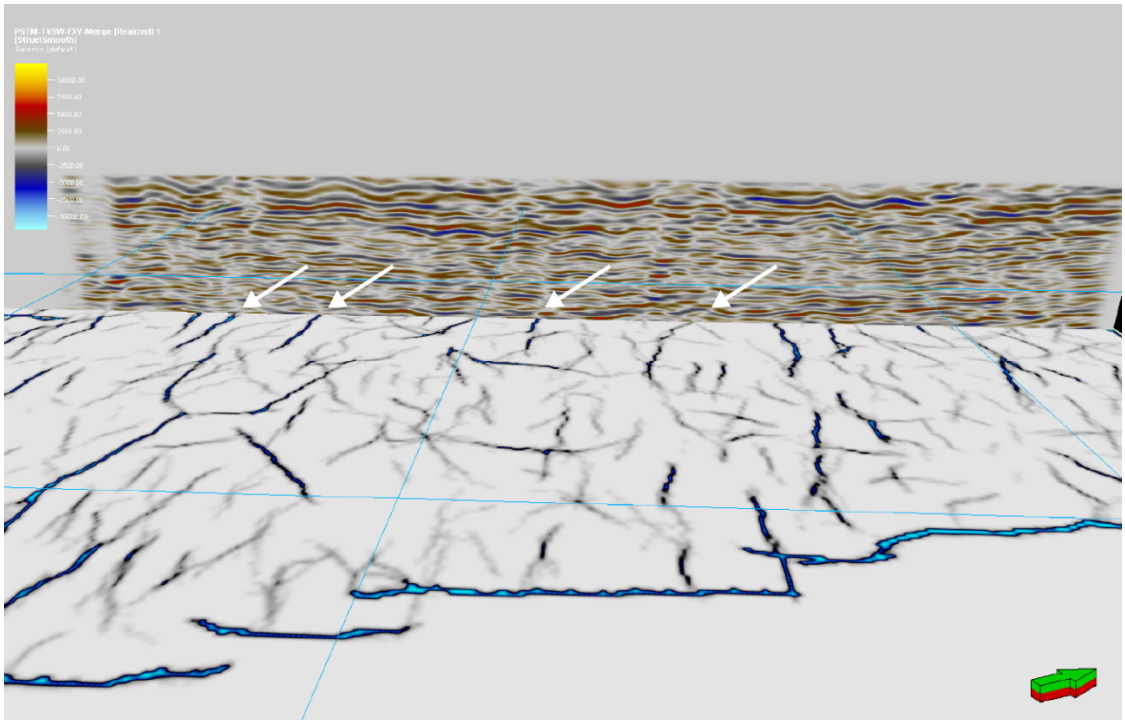

Figure 9. In the 3D window, we QC to validate the fractures in the time slice (–380 msec) and seismic profile – 465 (strike line). The white arrows point to fractures visible in the seismic amplitude vertical section corresponding to fractures predicted in the ant-tracker time slice.

Figure 10 shows the dip azimuths and strike azimuths for the fractures extracted from the total ant-tracking volume (Figure 8). The dominant fracture strike direction is NE–SW (055 ± 20°), approximately parallel to the structural strike of the adjacent Eastern Cordillera Foothills (055°). In the total volume, which includes the Cusiana fault hanging wall and footwall, other secondary fracture orientations are less common and difficult to statistically differentiate. When the non-folded footwall volume is considered separately however, secondary fracture orientations are resolvable.

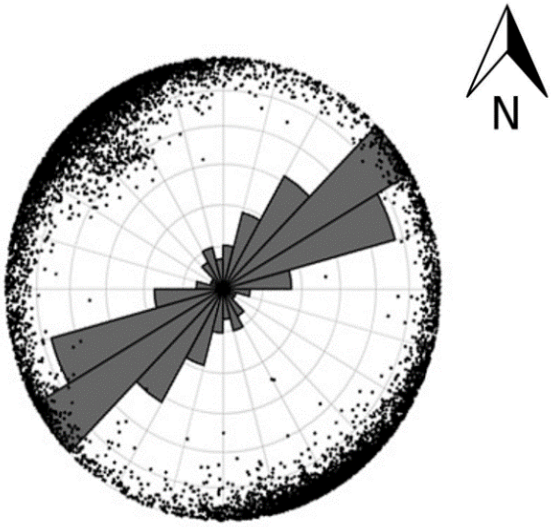

Figure 10. The rose diagram shows fracture dip azimuths (dark points) and fracture strike azimuths (rose petals).

4.2. Comparison of Fracture Systems in Folded and Non-Folded Rocks near the Cusiana Fault

In this study, we were able to compare the fracture intensity (relative number of fracture patch solutions) and orientation in folded rocks with the fracture intensity and orientation in non-folded rocks. The fracture orientations in the non-folded footwall block may help us to recognize the regional stress fields not associated with folding that are responsible for fracture formation. We divided the seismic volume into (1) folded units in the La Florida anticline in the hanging wall block of the Cusiana fault to the northwest and (2) non-folded units in the footwall block to the southeast. Basement, defined as pre-Late Cretaceous rocks (i.e., pre-Une Fm), were omitted from the seismic volume. Rose diagrams (Figure 11) show the dip azimuths and strike azimuths for fractures in the folded Cusiana fault hanging wall and the non-folded footwall. Fracture strike azimuths in the folded rocks of the hanging wall are predominantly NE–SW (055°), the main structural trend in the Foothills. No secondary orientations are distinguishable. Fracture strike azimuths in the non-folded rocks of the footwall (Figure 11) are also primarily NE–SW trending. However, an NNW–ESE secondary fracture strike orientation is also apparent. Schematic diagrams (Figure 11) show fracture types associated with folding [27]. The primary fracture orientation (NE–SW) is sub-parallel to the fold axis, the trend of type 2 or type 3 fracture sets [27]. Both type 2 and type 3 fracture sets are predicted for an elastic plate subjected to pure bending. The minimum principal stress direction during fracture formation was parallel to the fold dip direction and perpendicular to the fracture planes.

4.3. Secondary Fracture Orientations in Non-Folded Rocks of the Cusiana Footwall

The non-folded footwall block of the Cusiana thrust fault shows a NW–SE secondary fracture orientation. To highlight the secondary fracture orientations, we edited the ant-tracking attribute parameters to hide the primary NE–SW fracture sets with an "azimuthal filter" (Figure 12). The resulting filtered rose diagram (Figure 12) shows a prominent NNW–SSE (155 ± 15°) fracture strike trend. Another minor E–W (085 ± 10°) fracture trend is also visible. Both the NNW–ESE and E–W fracture trends are oblique (80° and 30°, respectively) to the regional foothills structural trend. They can be grouped as type 1 fracture sets [27] resulting from a vertical intermediate stress and maximum compressive stress parallel to the dip direction of bedding. Stearns (1968) [27] suggests that type 1 fractures form early during folding with the regional maximum compressive stress normal to the advancing mountain front.

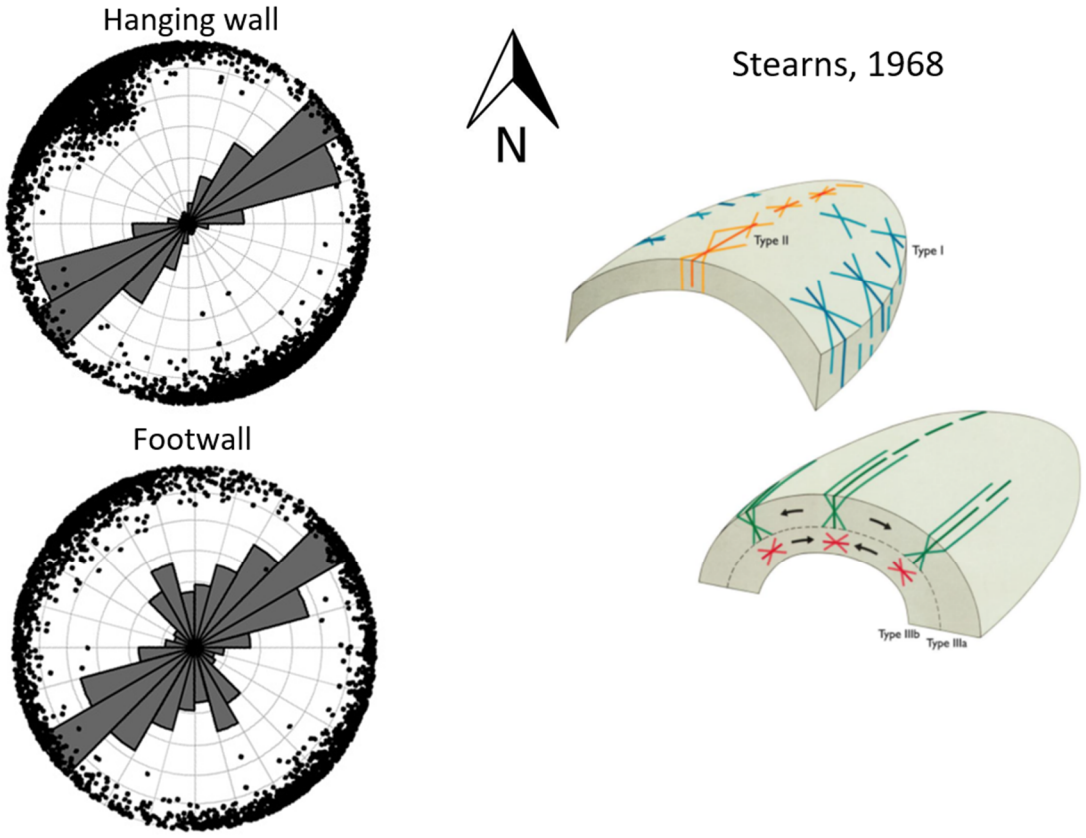

Figure 11. Rose diagrams (**left**) show the dip azimuths (dots) and strike azimuths (rose petals) for fractures in the Cusiana fault hanging wall and footwall. Schematic diagrams (**right**) show fracture types associated with folding (Stearns, 1968).

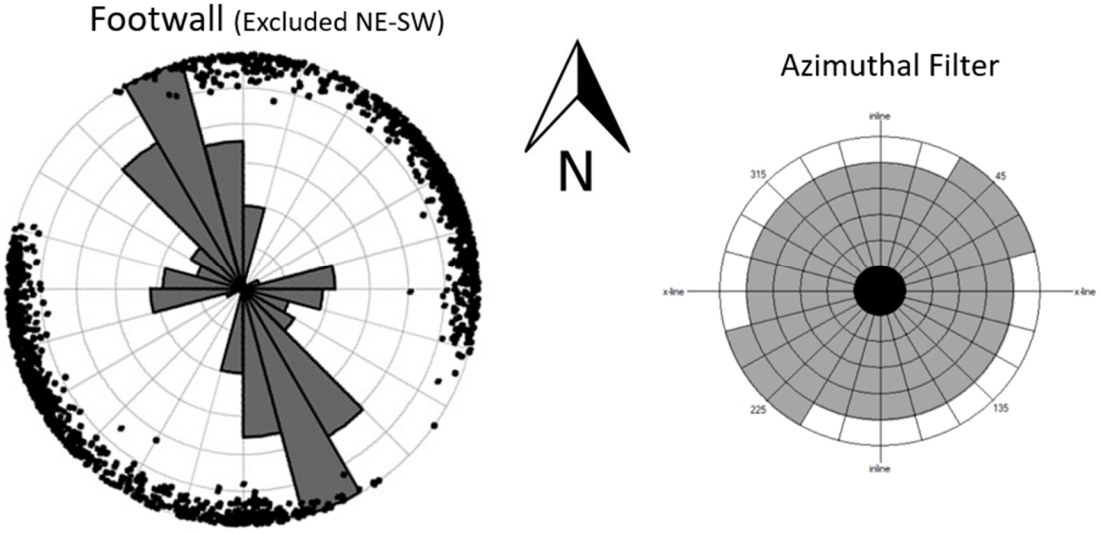

Figure 12. Rose diagram (**left**) after applying the azimuthal filter (**right**) to remove the dominant NE–SW striking orientation, forcing the artificial ants to detect fractures with secondary orientations.

4.4. Fracture Systems for the Guadalupe Group–Barco–Mirador Formation Reservoir Rocks

Understanding the orientation and spatial density of fractures where outcrops are sparse or absent is useful for modeling hydrocarbon flow, spatial density, fracture porosity, and fracture permeability in fractured reservoirs. In this study, we use a multi-attribute analysis of the La Florida 3D seismic volume using coherency and ant-tracking techniques for fault and fracture detection in reservoir rocks of the

Guadalupe Group, Barco Fm, and Mirador Fm. We were able to isolate the reservoir fractures (Figure 13) by cropping the ant-tracking volume between the base of the Guadalupe Group and the top of the Mirador Formation. The insets (Figure 13) are ant-tracking rose diagrams showing the orientations of reservoir fractures in the hanging wall and footwall of the Cusiana fault. Only one fracture orientation is apparent in both the hanging wall and footwall, the NE–SW trend prominent throughout the sedimentary volume, 060° ± 15° in the hanging wall and 055° ± 15° in the footwall. The fracture intensity in the reservoir rock, as visually estimated from the relative numbers of fault/fracture patch solutions (Figures 8, 10 and 13), is low relative to the total sedimentary volume, and the spatial density of fractures is similar on the hanging wall and footwall of the reservoir level La Florida fault-bend fold (Figures 3b and 13). The primary fracture orientation (NE–SW) is sub-parallel to the fold axis, the trend of type 2 or type 3 fracture sets [27] predicted for an elastic plate subjected to pure bending. The minimum principal stress direction during type 2 or type 3 fracture formation was parallel to the fold dip direction and perpendicular to the fracture planes.

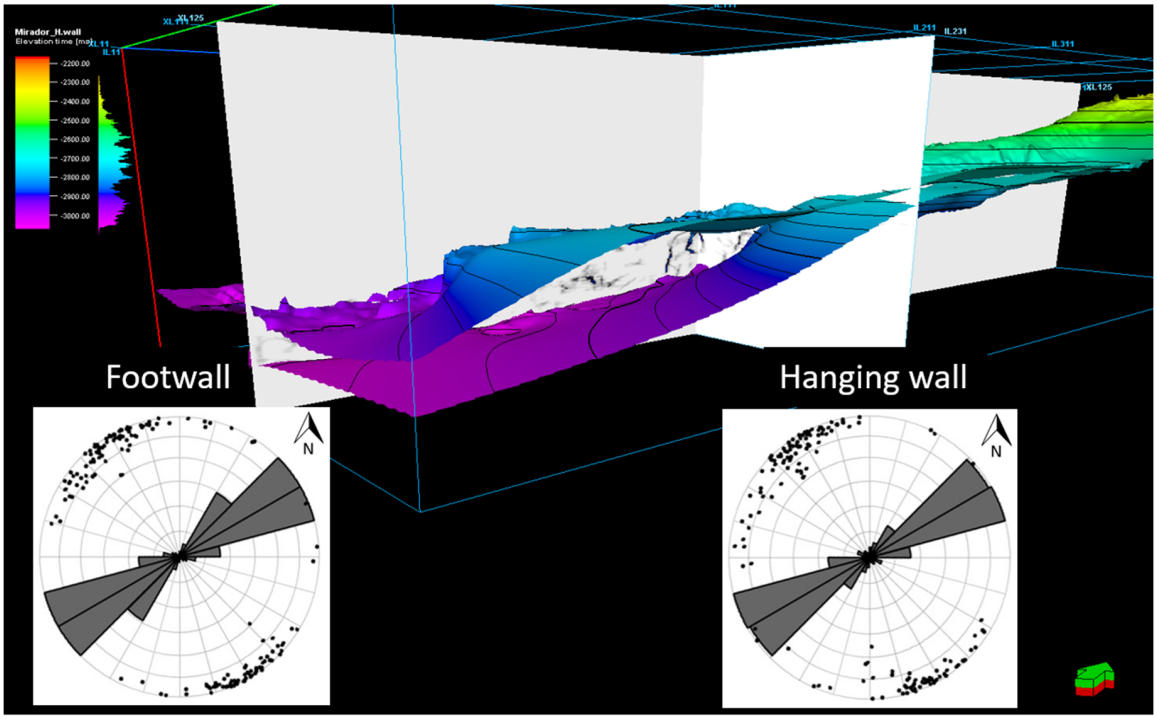

Figure 13. Ant-tracking data cropped between two surfaces to extract reservoir horizon fractures in Mirador Fm. The insets are rose diagrams showing the orientation of the Mirador Fm ant-tracking fractures in the hanging wall and the footwall.

4.5. Regional Stress Field—Timing and Orientation of Footwall Block Fractures

The fracture orientations in the non-folded footwall block may help us to recognize the regional stress fields not associated with folding that are responsible for fracture formation. If we can associate fractures with faults that show a measurable displacement, this will support regional stress field predictions and may also help determine the timing of fracture set formation.

4.5.1. Northeast–Southwest Trending Normal Faulting

Figure 14 shows a seismic amplitude profile and ant-tracking time slice at 1940 msec in the footwall block. The ant-tracking time slice reveals a NE–SW trending system of arcuate en-echelon fractures. The seismic profile demonstrates that the fractures form a normal fault system with a minor down-to-the-SE displacement. The displacement is a uniform downsection, indicating that it was not a growth fault. It dies out above 1000 msec TWT (Figures 5 and 14) in the lower Guayabo Formation

suggesting a 10 Ma late Miocene age, for faulting early in the latest Andean orogenic event. The NE–SW normal fault/fracture orientation indicates a NW–SE minimum principal stress direction and vertical maximum principal stress at the time of displacement. This is compatible with lithospheric loading by the advancing mountain front of the rising Eastern Cordillera.

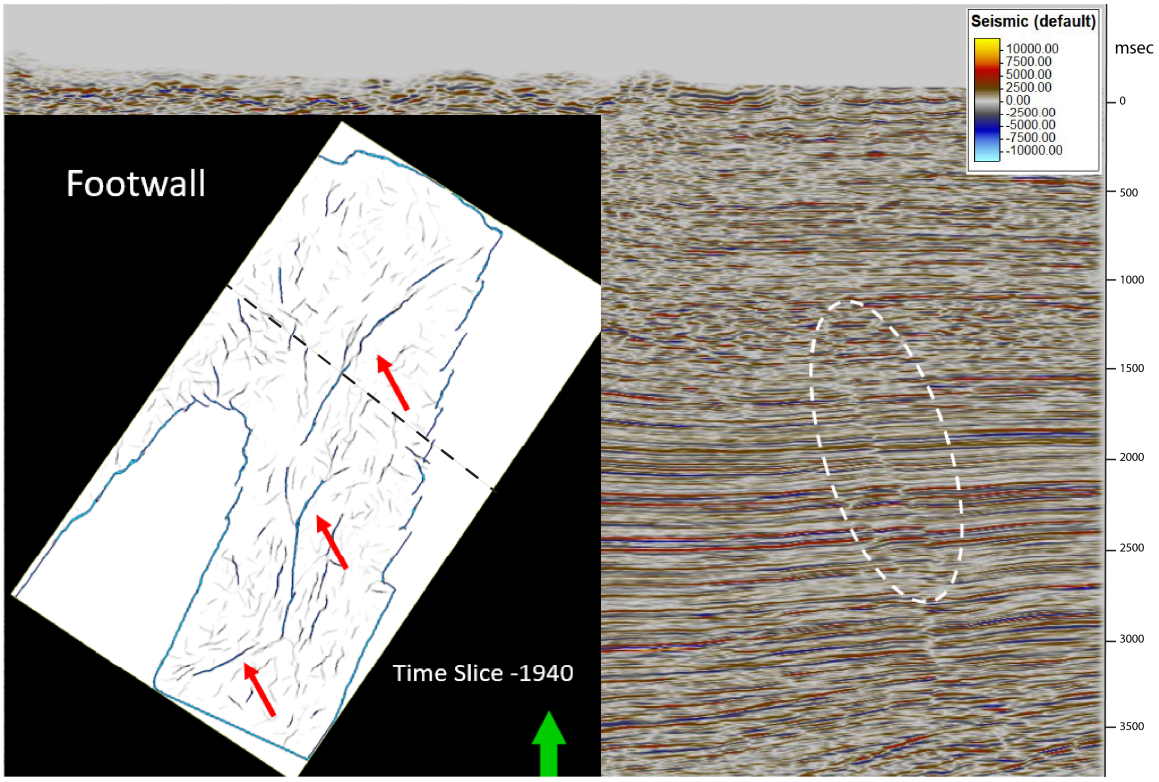

Figure 14. Seismic amplitude profile showing a normal fault (dashed white oval on the right), and the ant-tracking time slice (left) at 1940 msec showing the profile location (dashed black line) and en-echelon normal fault (red arrows).

4.5.2. Northwest–Southeast Trending Fracture Sets—Riedel shears?

An ant-tracker time slice at 380 msec in the footwall block (Figure 15) shows a prominent WNW–ESE (125° ± 5°) fracture set in the Guayabo Fm. Figure 9 shows that this fracture set corresponds to fractures observed in a seismic profile. Displacement cannot be determined from the seismic profile. However, we note that the intensity of WNW–ESE and NW–SE fracture sets is greatest in the sediments of the Guayabo Fm (11 Ma–Present) and hence roughly synchronous with the latest Andean tectonic phase. The least principal stress direction during at least part of this time period has been NE–SW, compatible with regional NW–SE maximum principal stresses during the formation of the advancing Eastern Cordillera Foothills. We also note a recent right-lateral displacement on the nearby Algeciras fault (Figures 1 and 16). The regional minimum principal stress direction for the Algeciras fault would also be NE–SW, and the NW–SE fracture sets could be interpreted as a Riedel shear set associated with this fault system. Riedel structures are networks of shear bands, commonly developed in zones of simple shear during the early stages of faulting [28].

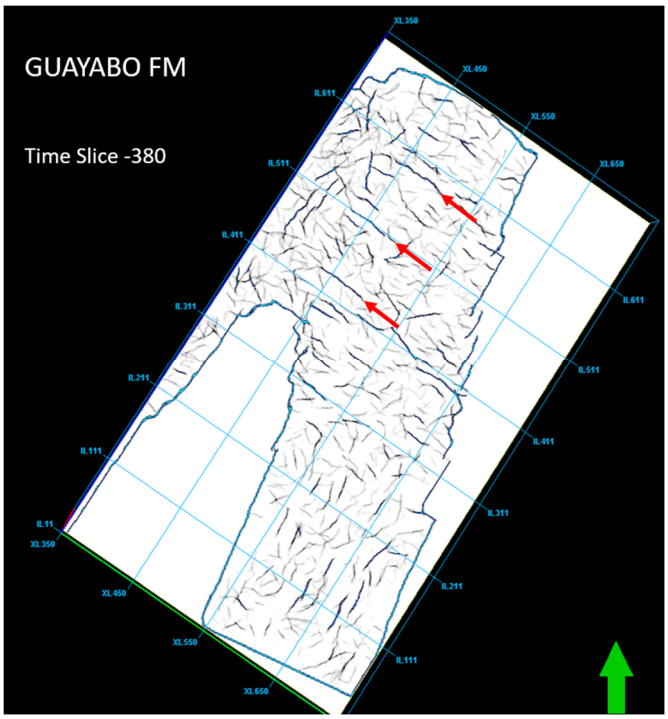

Figure 15. Time slice at 380 msec showing the WNW–ESE fracture direction in the Guayabo Fm in the footwall block.

5. Discussion

5.1. Comparison of Seismic Attribute Ant-Tracking Results with Previous Surface Mapping and Well Borehole Imager Log Results

Tamara et al. (2015) [3] published a comprehensive study of fractured reservoirs in the Eastern Foothills, focusing on their relationship with fold kinematics. These authors documented fracture orientations and related their distribution to fold geometries and folding mechanisms. Their study was based on the field mapping of outcrops to determine the relative timing of fracture sets, and subsurface borehole imager logs for the Cusiana, Cupiagua, and Piedemonte oil fields. Our study complements this work with the first multi-attribute analysis of a 3D seismic volume in the Foothills using coherency and ant-tracking techniques for fault and fracture detection. In this study, we compared the fracture intensity and orientation in folded rocks with the fracture intensity and orientation in non-folded rocks. The fracture orientations in the non-folded seismic volume helped us recover the regional stress field responsible for non-fold related fracture formation. Furthermore, we included the entire post-rift sedimentary volume above the pre-Late Cretaceous "basement", so that we were able to predict the relative timing and orientation of several fracture sets.

Tamara et al. (2015) [3] found four fracture sets in the Foothills folded reservoir rocks from surface mapping and well data: NE–SW, NW–SE, E–W, and N–S. Our study confirmed the first three of these sets in the seismic volume using attribute analysis: NE–SW, NW–SE, and E–W.

Figure 16. Topographic map with structural elements of the southeastern flank of the Eastern Cordillera and Llanos basin. Note the proximity of the Algeciras fault to the study area (white box, Figure 1).

The Cusiana oil field is located just 15 km to the northeast of the La Florida anticline along structural strike. Using well data, Tamara et al. (2015) [3] note that the NE–SW fracture set is present everywhere in the Cusiana reservoir rocks, with high intensities in the hinge region of the anticline. They also correlate the general fracture distribution with changes in the structural style in the Cusiana anticline along strike. The ant-tracking fracture results for the Guadalupe Group, Barco, and Mirador formations in the La Florida anticline, as well as the non-folded reservoir rocks to the SE (Figure 13), also reveal the prominent NE–SW fracture set. Our study was not able to resolve NW–SE, E–W, or N–S

fracture sets in the reservoir units, although the depth may limit the resolution of the seismic attribute analysis. We also noted that the fracture intensities (numbers of fracture dip azimuth solutions) in the folded La Florida reservoir units were visually similar to the fracture intensities in the non-folded reservoir units (Figure 13).

Our fracture orientations in the whole post-rift non-folded seismic volume suggest that regional stresses, as well as folding, could produce the NE–SW, NW–SE, and E–W fracture sets. In particular, late Miocene (10–9 Ma) NE–SW normal faulting may have been produced by lithospheric bending as the mountain front advanced from the northwest. However, in the whole volume, the NE–SW fracture intensity is greater in the folded rocks than in the non-folded footwall.

5.2. Algeciras Fault System, Regional Shear Stresses, and NW–SE and WNW–ESE Fracture Sets

The NW–SE and WNW–ESE fracture sets (Figures 9 and 15) are only found in the Guayabo Fm (11 Ma–Present) synchronous with the greatest orogenic shortening [29]. The regional NW–SE maximum principal stress that produced the orogenic shortening in the Foothills also produced the nearby right-lateral Algeciras fault system (Figure 16) [29]. The Garzón/Algeciras fault system has accommodated both dip-slip and strike-slip displacements in Miocene–Pliocene times [30]. In the Garzón Massif, Saeid et al. (2017) [31] demonstrated 10 to 17 km of northwestward thrust faulting over Miocene sediments for the Garzón/Algeciras fault system. Egbue and Kellogg (2010) [30] and Anderson et al. (2016) [32] proposed a transition from shortening to strike-slip deformation along the Garzón/Algeciras fault system approximately 2 m.y. ago. Using Landsat TM digital images, Chorowicz et al. (1996) [33] and Velandia et al. (2005) [34] estimated 3 to 5 km of right lateral shear in the last 2 Myr. on the Algeciras fault system. Right-lateral strike-slip displacement on the Algeciras fault system [30] could have generated N–S and WNW–ESE Riedel-type shear fractures in the Foothills study area.

6. Conclusions

Previous studies of fracture systems in the Eastern Cordillera Foothills have related their distribution to fold types and geometries based on field mapping and subsurface borehole imager logs. In the Llanos foothills, high levels of deformation have produced considerable noise in the seismic data, and as a result seismic attribute analysis has not been commonly used. In this paper, we present techniques to reduce noise and enhance seismic quality, making possible the first multi-attribute analysis of a 3D seismic volume in the Foothills using coherency and ant-tracking techniques for fault and fracture detection. In this study, we compared the fracture intensity and orientation in folded rocks with the fracture intensity and orientation in non-folded rocks. The fault patches volume clearly shows a greater fracture intensity in the folded Cusiana hanging wall than in the non-folded footwall. The dominant fracture strike direction is NE–SW (055 ± 20°), approximately parallel to the structural strike of the adjacent Eastern Cordillera Foothills (055°). For the Foothills fold and thrust belt, these fractures are parallel to the intermediate stress direction and perpendicular to the maximum principal stress direction. The ant-tracking fracture results for the reservoir rocks, the Guadalupe Group, Barco, and Mirador formations, in the La Florida anticline, as well as in the non-folded reservoir rocks to the SE, also reveal the NE–SW fracture set.

The fracture orientations in the non-folded seismic volume helped us recover the regional stress field responsible for non-fold related fracture formation. Our fracture orientations in the whole post-rift non-folded seismic volume suggest that regional stresses as well as folding could produce the NE–SW, NW–SE, and E–W fracture sets. The NE–SW trending type 2 and type 3 fracture sets are predicted for an elastic plate subjected to pure bending. Late Miocene (10–9 Ma) NE–SW normal faulting may have been produced by lithospheric bending as the mountain front advanced from the northwest.

To highlight secondary fracture orientations, we edited the ant-tracking attribute parameters to hide the primary NE–SW fracture sets with an "azimuthal filter". The resulting filtered rose diagram shows a prominent NNW–SSE (155 ± 15°) fracture strike trend and another minor E–W (085 ± 10°) fracture trend. Both the NNW–ESE and E–W fracture trends are oblique (80° and 30°, respectively)

to the regional foothills structural trend. They can be grouped as type 1 fracture sets [27] resulting from a vertical intermediate stress and maximum compressive stress parallel to the dip direction of bedding. The NW–SE and WNW–ESE fracture sets are only found in the Guayabo Fm (11 Ma–Present) synchronous with the greatest orogenic shortening. Right-lateral strike-slip displacement on the Algeciras fault system could have generated WNW–ESE Riedel-type shear fractures in the Foothills study area.

In this paper, we show the utility of coherency and ant-tracking techniques for the detection of fractures and faults in an active mountain foreland. The authors encourage further work to apply the method to a foreland structure, such as the Cusiana anticline, with both 3D seismic and borehole imager logs available. This could both validate and calibrate the coherency and ant-tracking method with well data as well as help visualize the complex 3D fracture patterns between wells. The resulting study could help reduce risk in 3D models of reservoir fracture porosity and permeability.

Author Contributions: Conceptualization, Z.A. and J.K.; methodology, Z.A.; software, Z.A.; validation, Z.A., I.H. and J.K.; formal analysis, Z.A.; investigation, Z.A.; resources, J.K.; data curation, Z.A. and E.S.; writing—original draft preparation, Z.A.; writing—review and editing, J.K. All authors have read and agreed to the published version of the manuscript.

Acknowledgments: This paper is a product of the first author's Ph.D. research at the School of Earth, Ocean, and Environment at the University of South Carolina. We would like to thank Frontera Energy (formerly Pacific Energy) for generously providing the 3-D seismic volume and well data for this research. Also, we would like to thank Obi Egbue, Andrew Leier, and David Barbeau for helpful discussions. Seismic interpretation software, Petrel 2019, was donated by Schlumberger. This research was supported by doctoral fellowships awarded to the first and third authors from King Abdulaziz City for Science and Technology (KACST), Riyadh - Saudi Arabia and a doctoral fellowship awarded to the fourth author from the Libyan Ministry of Higher Education and Scientific Research.

Conflicts of Interest: The authors declare no conflict of interest.

References

1. Cazier, E.C.; Hayward, A.B.; Espinosa, G.; Velandia, J.; Mugniot, J.F.; Leel, W.G., Jr. Petroleum geology of the Cusiana field, Llanos Basin foothills, Colombia. *Aapg Bull.* **1995**, *79*, 1444–1462.
2. Cooper, M.A.; Addison, F.T.; Alvarez, R.; Coral, M.; Graham, R.H.; Hayward, A.B.; Howe, S.; Martinez, J.; Naar, J.; Peñas, R. Basin development and tectonic history of the Llanos Basin, Eastern Cordillera, and middle Magdalena Valley, Colombia. *Aapg Bull.* **1995**, *79*, 1421–1442.
3. Tamara, J.; Mora, A.; Robles, W.; Kammer, A.; Ortiz, A.; Sanchez-Villar, N.; Piraquive, A.; Rueda, L.H.; Casallas, W.; Castellanos, J.; et al. Fractured reservoirs in the Eastern Foothills, Colombia, and their relationship with fold kinematics. *Aapg Bull.* **2015**, *99*, 1599–1633. [CrossRef]
4. Engelder, T.; Lash, G.G.; Uzcátegui, R.S. Joint sets that enhance production from Middle and Upper Devonian gas shales of the Appalachian Basin. *Aapg Bull.* **2009**, *93*, 857–889. [CrossRef]
5. Ortiz, A.; Mesa, G.D.; Beltran, R.X. Fracture modeling based on lithologic controls, geometry and tectonic evolution in the Llanos Foothills, Colombia. In Proceedings of the 2008 AAPG Annual Convention and Exhibition, San Antonio, TX, USA, 20–23 April 2008.
6. Mora, A.; Parra, M.; Strecker, M.R.; Sobel, E.R.; Zeilinger, G.; Jaramillo, C.; Da Silva, S.F.; Blanco, M. The eastern foothills of the Eastern Cordillera of Colombia: An example of multiple factors controlling structural styles and active tectonics. *Gsa Bull.* **2010**, *122*, 1846–1864. [CrossRef]
7. Albesher, Z.; Kellogg, J.; Hafiz, I.; Saeid, E. Structural Evolution of La Florida Anticline and Petroleum System in a Foreland Fold Belt, Eastern Cordillera Foothills, Colombia. In Proceedings of the 2019 AAPG Annual Convention and Exhibition, San Antonio, TX, USA, 19–22 May 2019.
8. Parra, M.; Mora, A.; Jaramillo, C.; Strecker, M.R.; Sobel, E.R.; Quiroz, L.; Rueda, M.; Torres, V. Orogenic wedge advance in the northern Andes: Evidence from the Oligocene-Miocene sedimentary record of the Medina Basin, Eastern Cordillera, ColombiaOrogenic wedge advance in the northern Andes, Colombia. *Gsa Bull.* **2009**, *121*, 780–800. [CrossRef]

9. Parra, M.; Mora, A.; Sobel, E.R.; Strecker, M.R.; González, R. Episodic orogenic front migration in the northern Andes: Constraints from low-temperature thermochronology in the Eastern Cordillera, Colombia. *Tectonics* **2009**, *28*. [CrossRef]
10. Teixell, A.; Ruiz, J.-C.; Teson, E.; Mora, A. The structure of an inverted back-arc rift: Insights from a transect across the Eastern Cordillera of Colombia near Bogotá. *Pet. Geol. Potential Colomb. Caribb. Margin: Aapg Spec. Vol.* **2015**, *108*, 499–516. [CrossRef]
11. Ramon, J.C.; Fajardo, A. *Sedimentology, Sequence Stratigraphy, and Reservoir Architecture of the Eocene Mirador Formation, Cupiagua Field, Llanos Foothills, Colombia*; The American Association of Petroleum Geologists: Tulsa, OK, USA, 2006; pp. 433–469. [CrossRef]
12. Toro, J.; Roure, F.; Bordas-Le Floch, N.; Le Cornec-Lance, S.; Sassi, W. *Thermal and Kinematic Evolution of the Eastern Cordillera Fold and Thrust Belt, Colombia*; The American Association of Petroleum Geologists: Tulsa, OK, USA, 2004; pp. 79–115. [CrossRef]
13. Reyes-Harker, A.; Ruiz-Valdivieso, C.F.; Mora, A.; Ramírez-Arias, J.C.; Rodriguez, G.; de la Parra, F.; Caballero, V.; Parra, M.; Moreno, N.; Horton, B.K.; et al. Cenozoic paleogeography of the Andean foreland and retroarc hinterland of ColombiaPaleogeography of the Northern Andes. *Aapg Bull.* **2015**, *99*, 1407–1453. [CrossRef]
14. Sánchez, N.; Mora, A.; Parra, M.; Garcia, D.; Cortes, M.; Shanahan, T.M.; Ramirez, R.; Llamosa, O.; Guzman, M. Petroleum system modeling in the Eastern Cordillera of Colombia using geochemistry and timing of thrusting and deformationPetroleum Systems Modeling Colombia. *Aapg Bull.* **2015**, *99*, 1537–1556. [CrossRef]
15. Parra, M.; Mora, A.; Jaramillo, C.; Torres, V.; Zeilinger, G.; Strecker, M.R. Tectonic controls on Cenozoic foreland basin development in the north-eastern Andes, Colombia. *Basin Res.* **2010**, *22*, 874–903. [CrossRef]
16. Carrillo, E.; Mora, A.; Ketcham, R.A.; Amorocho, R.; Parra, M.; Costantino, D.; Robles, W.; Avellaneda, W.; Carvajal, J.S.; Corcione, M.F. Movement vectors and deformation mechanisms in kinematic restorations: A case study from the Colombian Eastern Cordillera. *Interpretation* **2016**, *4*, T31–T48. [CrossRef]
17. Bande, A.; Horton, B.K.; Ramirez, J.C.; Mora, A.; Parra, M.; Stockli, D.F. Clastic deposition, provenance, and sequence of Andean thrusting in the frontal Eastern Cordillera and Llanos foreland basin of Colombia. *Geol. Soc. Am. Bull.* **2012**, *124*, 59–76. [CrossRef]
18. Chopra, S. Interpreting fractures through 3-D seismic discontinuity attributes and their visualization. *Cseg Rec.* **2009**, *34*, 5–14.
19. Matthäi, S.K.; Belayneh, M. Fluid flow partitioning between fractures and a permeable rock matrix. *Geophys. Res. Lett.* **2004**, *31*. [CrossRef]
20. Chopra, S.; Marfurt, K.J. Seismic attributes for prospect identification and reservoir characterization. In *Seismic Attributes for Prospect Identification and Reservoir Characterization*; Hill, S.J., Ed.; Society of Exploration Geophysicists and European Association of Geoscientists and Engineers: Tulsa, OK, USA, 2007; pp. 1–464. [CrossRef]
21. Liner, C.; Li, C.F.; Gersztenkorn, A.; Smythe, J. SPICE: A new general seismic attribute. In *SEG Technical Program Expanded Abstracts 2004*; Society of Exploration Geophysicists: Tulsa, OK, USA, 2004; pp. 433–436. [CrossRef]
22. Marfurt, K.J. Seismic Attributes as the Framework for Data Integration Throughout the Oilfield Life Cycle. In *Seismic Attributes as the Framework for Data Integration Throughout the Oilfield Life Cycle*; Society of Exploration Geophysicists: Tulsa, OK, USA, 2018; pp. 459–477. [CrossRef]
23. Singh, S.K.; Abu-Habbiel, H.; Khan, B.; Akbar, M.; Etchecopar, A.; Montaron, B. Mapping fracture corridors in naturally fractured reservoirs: An example from Middle East carbonates. *First Break* **2008**, *26*.
24. Randen, T.; Sønneland, L.; Carrillat, A.; Valen, T.S.; Skov, T.; Pedersen, S.I.; Rafaelsen, B.; Elvebakk, G. Preconditioning for optimal 3D stratigraphical and structural inversion. In Proceedings of the EAGE 65th Conference & Exhibition, Stavanger, Norway, 2–5 June 2003.
25. Pedersen, S.I.; Randen, T.; Sonneland, L.; Steen, Y. Automatic fault extraction using artificial ants. In *SEG Technical Program Expanded Abstracts 2002*; Society of Exploration Geophysicists: Tulsa, OK, USA, 2002; pp. 512–515. [CrossRef]
26. Wells, N.A. Are There Better Alternatives to Standard Rose Diagrams? *J. Sediment. Res.* **2000**, *70*, 37–46. [CrossRef]
27. Stearns, D.W. *Certain Aspects of Fractures in Naturally DEFORMED Rocks, in Rock Mechanics Seminar: Bedford*; Riecker, R.E., Ed.; Terrestrial Sciences Laboratory: Greenbelt, MD, USA, 1968; pp. 97–118.

28. Riedel, W. Zur Mechanik Geologischer Brucherscheinungen: Zentral-blatt fur Mineralogie. *Geol. Und Paleontol.* **1929**, 354–368.
29. Egbue, O.; Kellogg, J.; Aguirre, H.; Torres, C. Evolution of the stress and strain fields in the Eastern Cordillera, Colombia. *J. Struct. Geol.* **2014**, *58*, 8–21. [CrossRef]
30. Egbue, O.; Kellogg, J. Pleistocene to Present North Andean "escape". *Tectonophysics* **2010**, *489*, 248–257. [CrossRef]
31. Saeid, E.; Bakioglu, K.B.; Kellogg, J.; Leier, A.; Martinez, J.A.; Guerrero, E. Garzón Massif basement tectonics: Structural control on evolution of petroleum systems in upper Magdalena and Putumayo basins, Colombia. *Mar. Pet. Geol.* **2017**, *88*, 381–401. [CrossRef]
32. Anderson, V.J.; Horton, B.K.; Saylor, J.E.; Mora, A.; Tesón, E.; Breecker, D.O.; Ketcham, R.A. Andean topographic growth and basement uplift in southern Colombia: Implications for the evolution of the Magdalena, Orinoco, and Amazon river systems. *Geosphere* **2016**, *12*, 1235–1256. [CrossRef]
33. Chorowicz, J.; Chotin, P.; Guillande, R. The Garzon fault: Active southwestern boundary of the Caribbean plate in Colombia. *Geol. Rundsch.* **1996**, *85*, 172–179. [CrossRef]
34. Velandia, F.; Acosta, J.; Terraza, R.; Villegas, H. The current tectonic motion of the Northern Andes along the Algeciras Fault System in SW Colombia. *Tectonophysics* **2005**, *399*, 313–329. [CrossRef]